46th AIAA/ASME/SAE/ASEE Joint Propulsion Conference & Exhibit
25 - 28 July 2010, Nashville, TN

AIAA 2010-6662

46th AIAA/ASME/SAE/ASEE Joint Propulsion Conference & Exhibit, 25-28 July 2010, Nashville, TN

Improvements in Nanoparticle Dispersion Methods for Solid Propellants

David A. Reese* and Steven F. Son†
Purdue University, West Lafayette, IN, 47907, USA

Naida M. Lačević‡
NextGen Aeronautics, Torrance, CA, 90505, USA

Darren L. Naud§
DMD Systems, Los Alamos, NM, 87544, USA

Several numerical and experimental techniques for determining the state of dispersion of a nanoparticle-containing composite system are presented. The numerical investigations range in scale from molecular to mesoscale, using a combination of molecular dynamics and dissipative particle dynamics simulations to determine mix behavior. Experiments were performed to validate these numerical models and determine suitable mixing techniques for creating a disperse nanoparticle composite. In concert, the numerical and experimental results illuminate several pathways for improvements in solid propellant nanoparticle dispersion, including variations in mass fraction, input mixing energy, and particle coating.

I. Introduction

NANOPARTICLES HAVE long shown promise for increasing the performance of solid propellants. From early investigations illustrating potential combustion efficiency improvements, to later experiments focused on increased burning rate and improved agglomeration characteristics, nanoparticles present tantalizing possibilities for advances in solid propellant technology.[1–3]

Such advances, however, have been hampered by the extremely small size of the particles. The extremely high surface area of nanoparticles makes the inclusion of such material no simple task, especially in the relatively high viscosity binders popular in rocket motors today; the particles effectively "soak up" the binder, thus preventing high solids loadings from being achieved. Additionally, the nanoparticles are small enough that interaction forces between them create agglomerates which are difficult to disperse into the binder matrix. These agglomerates can be on the micron scale, thus negating most benefit provided by the nanoparticles.

In this paper, we present recent improvements in technology for dispersion of nanoparticles in solid propellant systems. A numerical model was developed and correlated with experimental data to determine the tendency for agglomeration in a mixture based on the mixing energy delivered to the system, and tested on three types of nanoparticles (aluminum nanopowder, boron nanopowder, and copper oxide nanorods) in binder systems of hydroxyl-terminated polybutadiene as a pseudopropellant. Each system was prepared using standard propellant mixing techniques to determine if a deagglomerated system could be achieved. The dispersion state of each system was characterized using post-mix viscometry, scanning electron microscopy (SEM), and small-angle x-ray scattering techniques. Additional techniques for incorporating nanoparticles in propellant are also presented.

*Graduate Student, School of Aeronautics and Astronautics, 500 Allison Rd., W. Lafayette, IN 47907, AIAA Member. Email: reesed@purdue.edu

†Associate Professor, School of Mechanical Engineering, 500 Allison Rd., W. Lafayette, IN 47907, AIAA Member. Email: sson@purdue.edu

‡Lead Engineer, 2780 Skypark Dr., Torrance, CA 90505.

§CEO, PO Box 635, Los Alamos, NM 87544.

II. Numerical Modeling & Simulations

Modeling work for this experiment was particularly challenging, as it involved interactions across a wide range of scales. Accordingly, molecular dynamics (MD) simulations were used to characterize the nature of nanoparticle/nanoparticle and nanoparticle/polymer interactions. The results of these simulations were applied to parameterize mesoscale simulations using dissipative particle dynamics (DPD) simulations to allow examination of the agglomerate microstructure behavior.

A. Development of Molecular Dynamics Models

Hydroxyl-terminated polybutadiene (HTPB) was chosen for this work, as it is a well-researched model binder in the computational energetic materials community. The HTPB polymer chain was built in the molecular dynamics simulation using chains of repeated monomers assembled into a "melt" simulation cell (see Fig. 1). Each cell contained 10 chains, which allowed for measurements of density, radius of gyration, radial distribution function (RDF), and mean-square displacement (MSD). These quantities were used to determine system equilibration in both structure and dynamics.

(a) (b) (c)

Figure 1: (a) 1,3 butadiene (monomer of polybutadiene); (b) Single chain of HTPB (hydrogen atoms are shown explicitly as light gray spheres, carbon atoms are displayed in dark gray and oxygen atoms are shown in red); (c) A snapshot from an MD simulation cell with HTPB chains.

Two types of molecular force fields exist to simulate HTPB via classical MD methods: united atom, and explicit atom. United atom force fields group nearby atoms into single particles, whereas explicit atom force fields describe the motion of each atom independently. Explicit atom fields provide greater accuracy; however, due to this level of granularity, their implementation is quite computationally expensive. More information on the benefits and drawbacks of each force field model may be found in Smith.[4] After a review of available literature on force fields for polybutadiene systems,[5–8] it became apparent that united atom force fields would produce sufficient accuracy for the molecular dynamics work. The Sandia LAMMPS software[9] was used for the simulations of polymer/polymer and polymer/nanoparticle interactions.

Structural and dynamical quantities, including density ρ, radius of gyration R_g, and radial distribution function $g(r)$, were first calculated for neat liquid HTPB systems over a range of molecular weights M_w (Table 1) at a temperature of 298 K and pressure of 0 Pa. Since the system is well-equilibrated, ρ is relatively constant as M_w increases, suggesting that polymer chain packing is not affected by chain length for this M_w regime. The variation in ρ as a function of M_w is shown in Fig. 2a.

Figure 2b shows the average radius of gyration R_g for the polymer chains as a function of M_w. As M_w increases, R_g increases until an effective "saturation" is achieved at $M_w \approx 2800$ g/mol. Whereas density gives a measure of the overall packing efficiency of the system, radius of gyration describes the conformation of the individual polymer chains. Consequently, these quantities are important validation of the model for application to nanoparticle interaction studies. Both density and radius of gyration agree well with experimental values reported by Smith, et al.,[5] and references therein.

The static structure of the neat HTPB melt is further characterized via the radial distribution function, $g(r)$. This function measures the probability of finding two particles at distance r. It gives the radially

Table 1: Molecular weights for varying number of carbon atoms on HTPB model chains.

No. of C Atoms	M_w [g/mol]
60	840
120	1650
200	2800
240	3270
360	4890

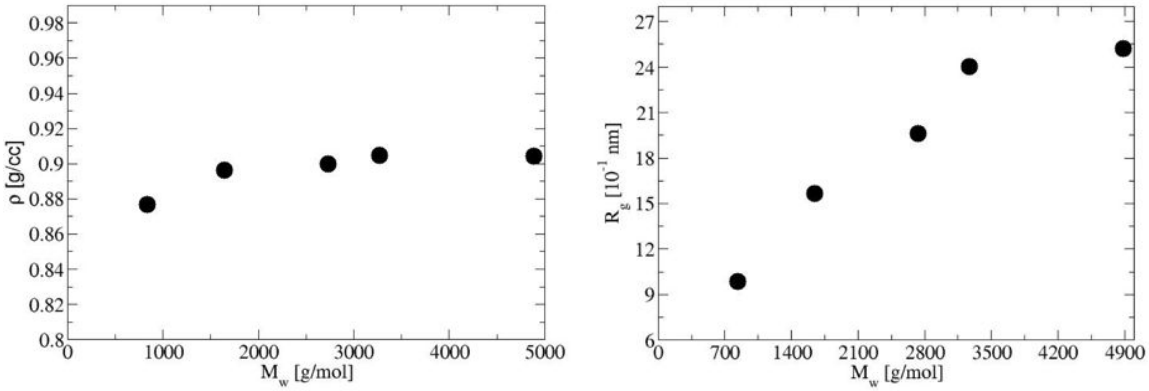

(a) $\rho\,(M_w)$ (b) $R_g\,(M_w)$

Figure 2: Initial results of molecular dynamics simulations for neat HTPB.

averaged atomic coordination, and is expressed mathematically as

$$g(r) = \frac{1}{\rho N} \sum_{i,j}^{N} \delta\left(r - r_{i,j}\right) \ , \tag{1}$$

where δ is the Dirac delta function, ρ is the density of the system, N is the number of particles in the system, and $r_{i,j}$ is the distance between particles i and j. Figure 3 shows $g(r)$ between carbon atoms in HTPB, $g^{\mathrm{C-C}}(r)$, and the inset shows $g(r)$ between OH groups, $g^{\mathrm{OH-OH}}(r)$. $g^{\mathrm{C-C}}(r)$ is characterized with four distinct peaks that correspond to characteristic distances between first, second, third, and fourth nearest carbon atoms along the HTPB chain. The positions of the peaks are consistent with $g(r)$ computed by Li and Mattice[10] for a similar system. Since far fewer OH-OH interactions exist, the inset $g^{\mathrm{OH-OH}}(r)$ data is necessarily noisier, however a distinct peak is clearly visible at $r \approx 0.5$ nm. This gives an indication of the OH-OH coordination which can be used in studies of polyurethane formation, where strong activity of the terminal groups is important to crosslinking. $g(r)$ is particularly useful, as it is the Fourier transform of the structure factor $S(q)$, which is a quantity that can be obtained from x-ray scattering experiments (e.g., SAXS).

Additional kinetic properties of the neat HTPB system were also investigated to validate the model and provide parameterization for DPD. The Mean Square Displacement (MSD), defined as $< r^2(t) >$, was calculated to enable calculation of the diffusion constant D of the system. MSD and D are related by the Einstein law for a three-dimensional system:

$$< r^2(t) > = 6Dt \tag{2}$$

where t is the elapsed time. The results of MSD calculations and the resulting values of D are shown in Fig.s 4a and 4b, respectively. D is an important characteristic of the system to track, as it is directly related to its viscosity and dispersion characteristics. Figure 4 provides insight into the effect of binder molecular weight on the basic physical processes involved in nanoparticle dispersion. As molecular weight increases, the diffusion characteristics change suddenly at approximately 2000 g/mol; the HTPB used in the experimental

validation has a molecular weight of 2800 g/mol, placing it in the secondary diffusion regime, and making it better suited to processing with particles on the micro-scale.

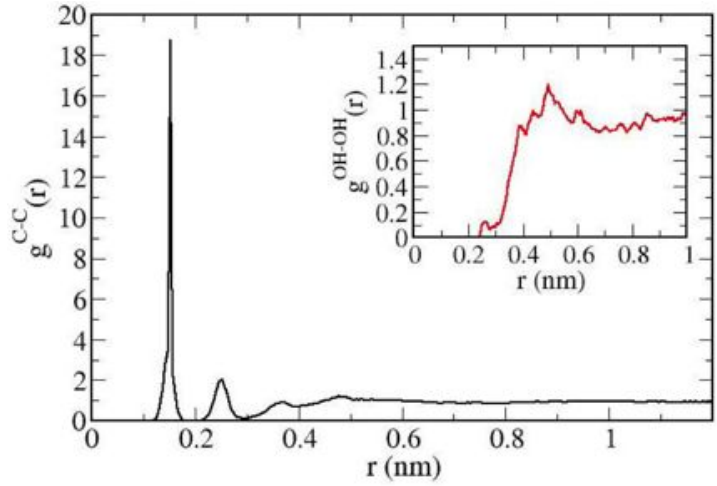

Figure 3: Radial distribution functions $g^{\mathrm{C-C}}(r)$ and $g^{\mathrm{OH-OH}}(r)$ (inset) for HTPB $M_w = 2740$ g/mol and a temperature of 298 K.

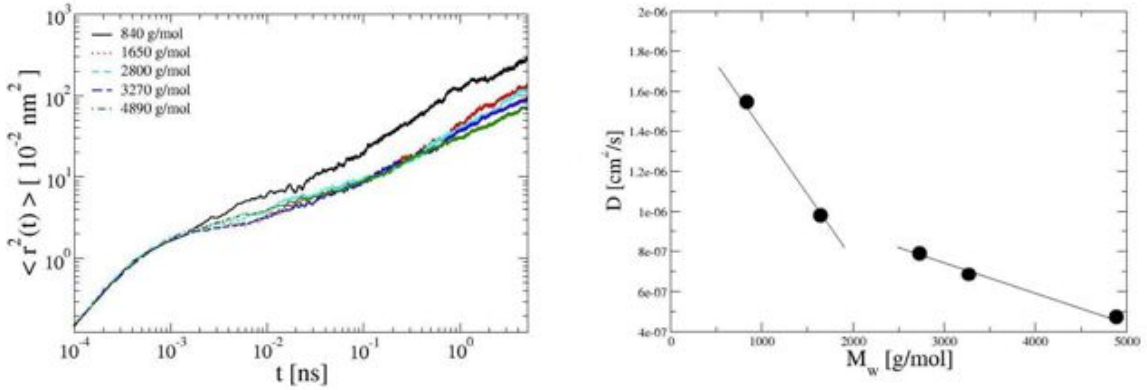

(a) (b)

Figure 4: (a) Mean square displacement (MSD) and (b) diffusion constant D of HTPB for varying molecular weights. Note the crossover in diffusion regimes at 2000 g/mol.

B. Molecular Dynamics Simulations

With a well-established HTPB model, nanoparticle interactions were incoprated into the simulations. A 5 nm diameter aluminum particle was introduced into the HTPB cell to determine surface interactions between the nAl oxide-coated surface and HTPB (Fig. 5). The force field interaction parameters between the surface of the nAl particle and HTPB calculated by Jin, et al.[11] were used. The normalized density profile (Fig. 5b) shows a well ordered interfacial region ∼2 nm thick, where the particle/polymer interaction is dominant. For nanosize particles, the interfacial region plays a major role in the system, whereas for larger micron-size particles, this region would be far less dominant.

The surface interaction was likewise used to calculate the potential of mean force (PMF) between particles of several geometries (Fig. 6) as a function of separation distance r in the HTPB matrix. The results of the repulsive component of the PMF calculations are shown in Fig. 7.

It becomes apparent from the PMF calculations that, at spacings greater than approximately 10 nm, repulsion forces between the nanoparticles are extremely weak, and thus the nanoparticles tend to agglomerate

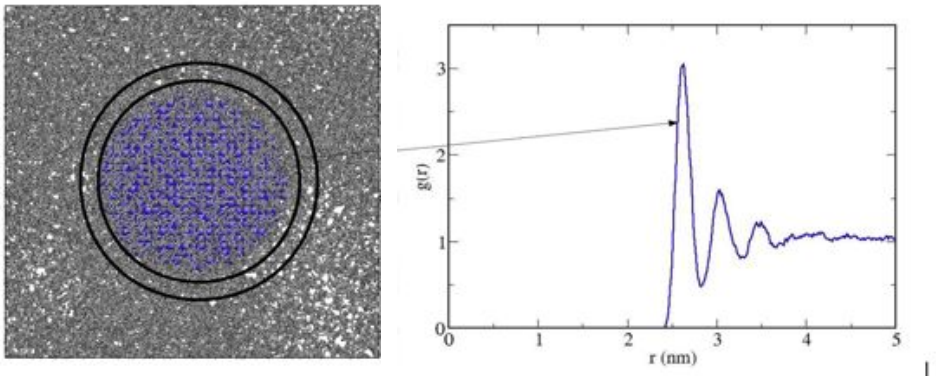

(a) (b)

Figure 5: (a) nAl in HTPB, with nearest neighbor shell denoted by black rings; (b) Normalized density profile of HTPB at interface with nAl as a function of distance from particle center. Interactions extend beyond 50% of the diameter of the nanoparticle from the surface.

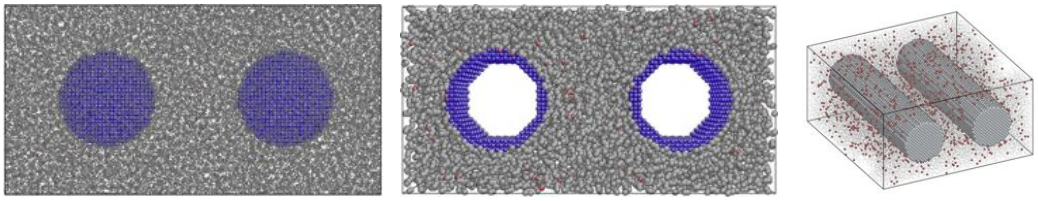

(a) (b) (c)

Figure 6: (a) 5 nm nAl spheres, (b) 5 nm × 20 nm nAl tubes, (c) 5 nm × 20 nm nAl rods in HTPB matrix for calculations of PMF.

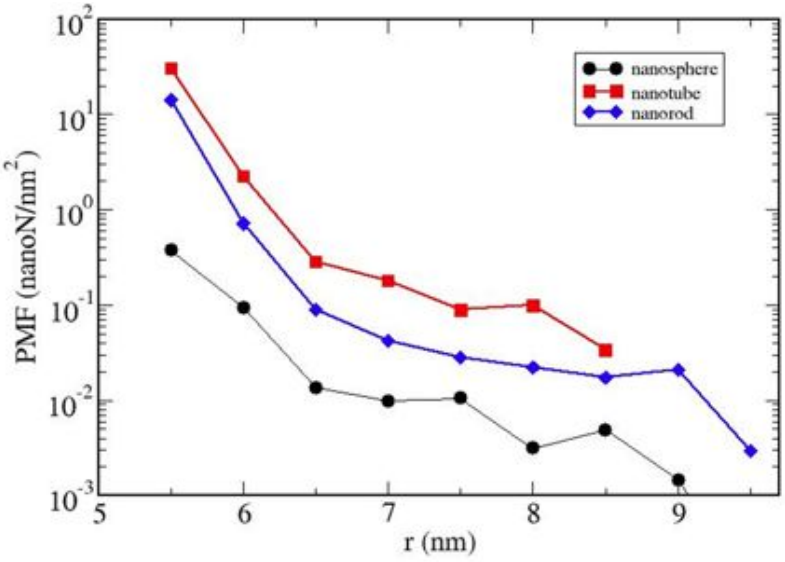

Figure 7: Plot of log(PMF) as a function of particle separation distance r for nanosize aluminum spheres, rods, and tubes.

on the molecular scale during mixing. Various surface treatments, including the behavior of "functionalized" nanoparticles and coated nanoparticles, are currently being investigated to improve the dispersion characteristics of the nanocomposite. Chemical dispersion methods may also be of assistance.

C. Dissipative Particle Dynamics Simulations

Since propellant processing happens on length and time scales significantly larger than that afforded by molecular dynamics simulations, the mesoscale method of dissipative particle dynamics (DPD) was implemented to allow consideration of lab-scale problems. The DPD method uses a force field f given by piecewise interactions, based on distance:

$$f = \begin{cases} \left(F^C + F^D + F^R\right)\hat{r}_{i,j} & r < r_c \\ 0 & r \geq r_c \end{cases} \tag{3}$$

where F^C, F^D, and F^R are conservative (elastic), dissipative, and random forces between the particles, respectively, $\hat{r}_{i,j}$ is the unit vector along the particle separation direction, and r_c is a critical radius beyond which the particles do not interact. The forces F are given by

$$F^C = Aw(r) \tag{4}$$

$$F^D = -\gamma w^2(r)\left(\hat{r}_{i,j} \cdot \overrightarrow{v}_{i,j}\right) \tag{5}$$

$$F^R = \sigma w(r)\alpha(dt)^{1/2} \tag{6}$$

where

$$w(r) = 1 - \frac{r}{r_c},\ r < r_c\ . \tag{7}$$

r_c is chosen based on the size of the mesoscale particles in order to produce a realistic averaging of interactions. For this work, r_c was chosen to encompass approximately 10^2 neighboring particles. A rough estimate of the parameters A and γ were obtained analytically using the method described by Español,[12] using measured values of viscosity and bulk modulus. Filler/filler interactions were assumed to be purely conservative with no viscous component, using the 9/6 Lennard-Jones potential. Filler/matrix interactions were expressed with a conservative and a viscous component, using Stokes' law to model the drag force of a filler particle moving at a constant velocity.

Once parameterized, the nanoscale DPD model provided the ability to examine the tendency for agglomeration of initially well-dispersed particles under mild agitation. This simulation essentially presents an upper bound for the degree of dispersion that can be expected for a given composite and input mixing energy. The results of this simulation for various mass fractions are shown in Fig. 8, with 25 nm diameter Al particles in an HTPB matrix and DPD parameters A = 8 nN and $\gamma = 0.8$ nN-sec/m.

Additionally, DPD modeling was used to calculate the RDF of the composite for various interaction strengths and mass fractions of particles, allowing direct comparison with experimental microstructure characterization. In this case, the RDF is acting as a measure of the state of agglomeration of the system.

Based on metrics of agglomeration from the DPD simulations, a diagram such as that shown in Fig. 9 can be created. Figure 9 is an extremely simple and powerful way to summarize results from both the MD and DPD simulations, as it illustrates the tendency of a given nanocomposite mixture to disperse or agglomerate as a function of mass fraction and energy input. Such a "phase diagram" may serve as a guide for the required interaction between particles to generate a well-dispersed system.

Although the size of agglomerates condensing from a well-dispersed state is useful for characterizing an ideal mixture, it does not properly describe the experimental mixing process. In the latter case, much larger agglomerates are broken up as mixing proceeds and mean agglomerate size is reduced. The mesoscale models developed can treat such interactions, and current work is focusing on the use of experimental microstructural information from SEM images to design simulations of realistic agglomerate collisions during mixing.

III. Experimental Process Development

The focus of this investigation was the suspension of fuel nanoparticles in an inert propellant binder, to simulate the future development of live propellants. Though the mixtures created were non-reactive, safety and processing challenges nonetheless occurred which required the development of a rigorous mixing and

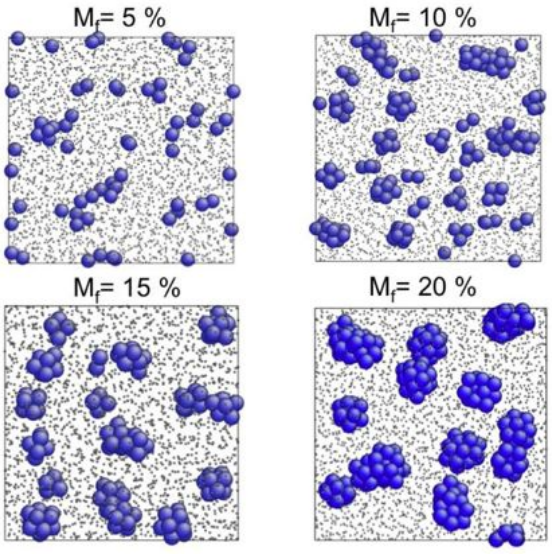

Figure 8: Snapshots from DPD simulations at several mass fractions M_f. nAl particles are displayed as blue clusters, and matrix particles are displayed as gray dots. Larger stable agglomerates are evident at higher mass fractions.

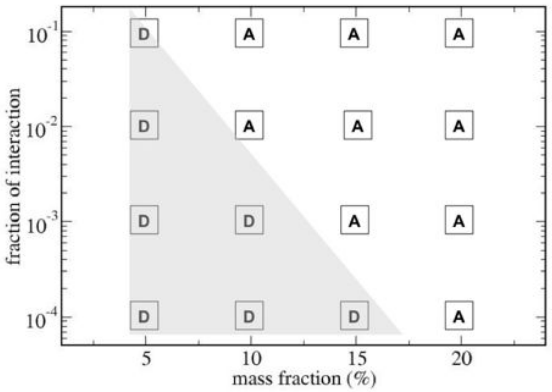

Figure 9: DPD mixing phase diagram, which provides approximate bounds for disperse/agglomerated systems.

Figure 10: Initial weighing of nanoaluminum (left), nanoboron (center), and Copper Oxide nanorods (right) in HTPB.

testing procedure. Each mix began by taking the tare weight of the mixing vessel (US Plastics p/n 70211) and adding 150g of hydroxyl terminated polybutadiene (HTPB) binder prepolymer to the jar. The appropriate amount of nanoparticles were then added atop the HTPB. Since potentially energetic nanoparticulate matter was involved in the processes, it was critical to insure that dusting of the nanoparticles did not occur. Dusting would create an extremely hazardous, static sensitive mixture of the fuel particles with air, presenting a significant explosion hazard. As such, following the weighing of nanoparticles into the binder, a wooden stir rod was used to push the particles into the mix, wetting them and preventing a dusting hazard. The compound was then ready for further mixing.

A. LabRAM Mixing Process

A resonant mixer (LabRAM, Resodyn Corportation, Butte, MT; Fig. 11) was used for particle dispersion. This mixer operates by oscillating the mixing jar vertically at varying frequencies to promote even distribution of the particles in the slurry. The LabRAM is equipped with an accelerometer and a control system designed to detect the resonant frequency of the composition. The LabRAM then automatically adjusts the mixing frequency to find and maintain the resonant frequency as the level of mixedness progresses.[13]

Figure 11: Resodyn LabRAM mixer.

As the mixing frequency is determined automatically by the mixer, the only variable that was adjusted was the mixing duration. The LabRAM mixer is unique in that it also records frequency and acceleration as a function of time to a computer data acquisition system; this output proved invaluable in determining the required mixing duration for the slurry. The recorded acceleration output for three concentrations of nanoparticle dispersion is shown in Fig. 12.

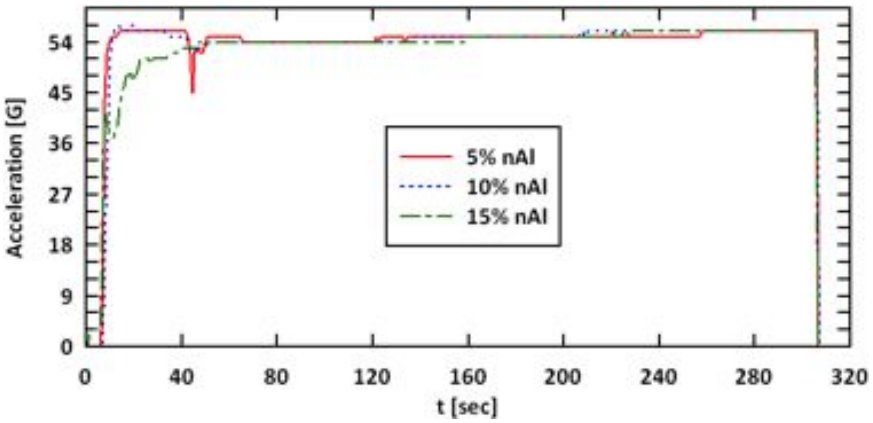

Figure 12: Time dependence of mix acceleration for three nanoparticle concentrations.

As can be seen in the figure, the mixing acceleration varies strongly as a function of time as the state of mixedness increases. After approximately 80 seconds, all mixes were close to a plateau in their acceleration values, indicating near completion of the mix. After 250 seconds, very little change occurs, and thus a five minute (300 second) mix duration was used for all mixes to provide some margin on mix completion.

The final developed mixing process was as follows:

1. Tare weighing jar on lab balance, noting tare weight.
2. Add 150g HTPB to jar.
3. Add nanomaterial to jar.
4. Wet out nanomaterial in HTPB using a wooden stick (anti-static, non-sparking).
5. Mix on LabRAM (60 G acceleration) for 5 minutes.

B. Sonication Process

Though this mixing process appeared to generate satisfactory results for the mixtures loaded with higher solids loadings, the low loading mixtures were noted to experience significant agglomeration, as can be seen in the sample from a 5% nAl mix in Fig. 13. This agglomeration led to the use of a Branson S-250D digital sonifier and sonic horn to disperse the particles before incorporation into the HTPB. To allow dispersion, solvent was added to the nanomaterial prior to the addition of HTPB in a 3:1 ratio by weight. This provided enough working room for the sonic horn to break up the agglomerated material and promote full dispersion of the particles. This solvent-particle slurry was then added to the HTPB and mixed on the LabRAM. The solvent was then removed by heating the mixture and placing it under a 1.6 kPa (absolute) vacuum.

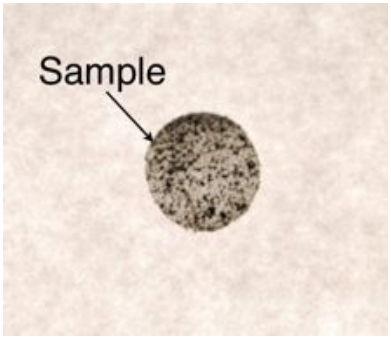

Figure 13: Microscale agglomeration of 5% nAl noted in a 10mm diameter sample.

The sonic horn intensity and duration was varied until a slurry of nanomaterial in the solvent was generated. The resulting process operated at an 80% duty cycle on for 80 ms, off for 20 ms to prevent excessive heating of the sample, 1 minute at a time, for a total of 5 minutes. The slurry was stirred quickly with a chemical spatula every minute between cycles, to insure dispersion of the entire sample. The resulting mixture was gel-like in rheology. This mixture was then added to the HTPB (see Fig. 14) and mixed on the LabRAM as discussed previously. Initially, n-hexane was used as the solvent, based on prior successful

Figure 14: Gel slurry of nAl and n-pentane added to HTPB for further mixing.

experience. However, the quality of the hexane solvent was called in to question when a waxy sheen, assumed to be paraffins, was noted atop the evacuated mixture. Additionally, the hexane-based mixture never returned to its pre-dispersion viscous state, indicating that some solvent still remained, even after several hours under vacuum at elevated temperatures (∼60 °C). These developments led to the selection of n-pentane as the solvent of choice for dispersion. Though the increased vapor pressure of n-pentane led to additional challenges in the form of reduced processing time, its ease of removal led to greater success in the mix process.

C. Crosslinking and Preparation for SEM/SAXS

It was desired to perform additional diagnostics on the mixture beyond simple liquid viscosity measurements to determine the state of agglomeration. The use of SEM and SAXS techniques would provide additional data, however they required a solid sample to be created. To create the stiffest sample possible, a modified methylenediphenyldiisocyanate crosslinker (Isonate 143L MDI) was chosen. The MDI family of isocyanates is based off of a symmetric aromatic chain structure, thus providing a stiffer finished product than if an asymmetric or aliphatic isocyanate (e.g., isophorone diisocyanate IPDI) was chosen.

The isocyanate was incorporated into the HTPB at the beginning of the mix process. The 143L MDI provided an approximately two hour working time, which proved to be sufficient to complete the mix. A NCO:OH ratio of 1.2 was used so as to promote maximum tensile strength of the polymer mixture. The 143L was weighed out with the HTPB for a total of 150 grams of liquid and premixed to insure full mixing of the crosslinker and the prepolymer. The mix then proceeded as previously outlined.After mixing on the LabRAM, the final product was laid out in forms comprised of Teflon-coated aluminum with wood siding (non-sparking) to allow control over the sheet thickness. To allow SAXS measurements to occur in transmission, 1mm thick sheets of polymer/nanomaterial were created, as seen in Fig. 15. These sheets were cured in an oven at 40 °C for 24 hours prior to stamping into 10mm diameter wafers with a circular cutter.

D. Sample Preparation

After development of the appropriate manufacturing steps, samples were prepared for further characterization. Each sample set was prepared in three weight percentages: 5% nominal (4.47% nanomaterial, 95.53% HTPB), 10% nominal (9.09% nanomaterial, 90.91% HTPB), and 15% nominal (13.04% nanomaterial, 86.96% HTPB). An additional sample was prepared using neat HTPB to provide a baseline viscosity measurement.

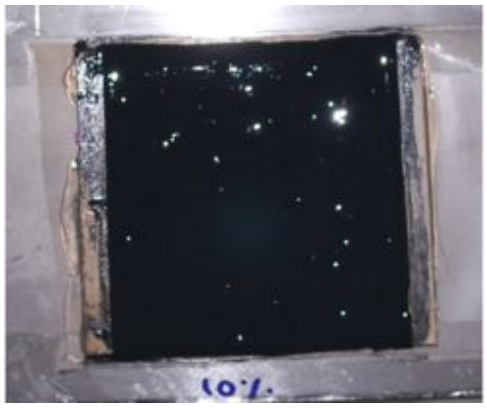

Figure 15: Crosslinked 10% nanoaluminum/HTPB sample cast in sheet mold.

The weight percentages of nanomaterial were chosen to represent typical percentages of metals (nAl, nB) and catalysts (nCuO) present in existing composite propellant formulations. According to thermochemical analysis performed on a standard 86% solids AP/Al/HTPB propellant using the NASA CEA code (see Fig. 16), delivered specific impulse maximizes near 16% aluminum concentration by weight; as such, a percentage near this was selected as an upper bound for the sample weights. An expansion ratio of 8 was assumed.

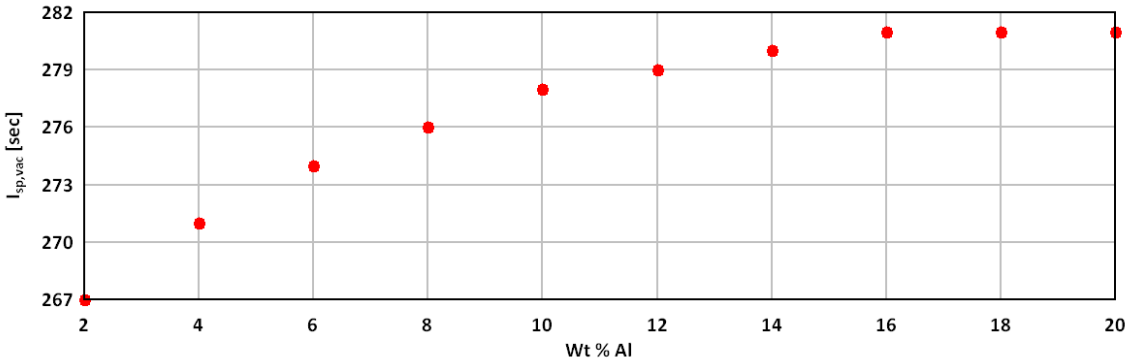

Figure 16: Data from NASA CEA ($\varepsilon = 8$, $P_c = 1000$ psi) showing dependence of delivered specific impulse on propellant aluminum content.

For each nanomaterial, all sample sets were manufactured simultaneously to ensure consistency in the mixing process environmental conditions. The initial viscosity measurement sample sets were generated with 150g of HTPB polymer base, as this was the minimum amount measurable by the Brookfield DV-II+ Pro HB viscometer used by this project. Each set of sample jars was weighed for consistency and cleaned prior to sample preparation.

1. Preparation of Neat HTPB System

The neat HTPB sample was prepared by placing 150 grams of R45M HTPB (Firefox Enterprises, Pocatello, ID) into a sample jar. R45M was chosen, as it is the military-specified version of R45; it differs from the other popular R45 prepolymer blend R45HT in its hydroxyl functional distribution and distribution of molecular weights. Though both materials have the same average molecular weight, R45M features more hexene-terminated chains, while R45HT emphasizes the vinyl and geraniol-terminated chains; the net result is an emphasis on mid-molecular weight molecules in the R45M, and a broader distribution in the R45HT. The bias towards hexene terminated chains results in a slightly lower viscosity for neat R45M.

For the neat R45M, no further processing beyond weighing of the sample was performed, as it was created to provide a baseline viscosity for the material without the inclusion of nanomaterial.

2. Preparation of Nanoaluminum Systems

The nanoaluminum propellant systems were prepared next, as, out of the materials planned, the Purdue laboratory has the most experience with preparation of nanoaluminum-based propellants. The nanoaluminum (80nm nominal diameter, Novacentrix, Austin, TX) is kept under a positive pressure inert argon environment to prevent further oxidation of the particles while in storage.

Two sets of three nanoaluminum samples each were generated for characterization; the first set was used for viscosity measurements, and included only nAl and HTPB. The second set was fabricated for x-ray and SEM characterization, and included nAl, HTPB, and Isonate 143L MDI as a crosslinking agent. The amount of liquids in each sample set remained fixed (150g) so as to ensure consistent particle interactions in the mixture. In each case, 150g of polymer base was weighed into the sample jar, followed by the nanoaluminum in 7.5g, 15g, and 22.5g amounts for the 5% nominal, 10% nominal, and 15% nominal cases, respectively. The aluminum powder was hand-wetted into the polymer base to prevent formation of a dust cloud in the LabRAM mixer, and the sample was then mixed using the RAM while recording acceleration values to monitor the state of mixedness, as outlined in the previous section.

Figure 17: Preparation of 5% and 15% nAl samples in HTPB, pre-wetting, with 143L MDI added.

The crosslinked samples were cast into sheet molds and held at 140 °F (40 °C) for 24 hours to promote crosslinking. Viscosity and temperature measurements were taken immediately after mixing on the RAM to prevent potential settling of the nanoaluminum from the mixture. Photos of the sample preparation process appear in Fig. 17. The nanoaluminum mixing process proceeded as planned.

Sonication was also attempted with the nanoaluminum-based systems as a method to break up the agglomerates noted in the lower mass fraction systems. As mentioned above, initial attempts with hexane left a paraffin residue atop the samples, and exhibited prohibitive difficulty in the removal of the hexane from the HTPB system. Pentane was then selected as a replacement solvent; samples were prepared with 15g of nAl sonicated in 45g pentane, then mixed on the LabRAM mixer and vacuumed to remove the solvent. This process proved successful in providing superior dispersion of the nanoaluminum particles; no agglomerates were visible in the final product.

3. Preparation of nCuO Systems

The nCuO rods were sourced from NEMS/MEMS Works LLC (Columbia, MO), and are 8-12 nm diameter, 100-150 nm in length, and have specific surface area 100-120 m^2/g. Initial mix attempts with the nCuO rods proved the difficulty of mixing particles of this unique shape. While wetting the particles by hand, the rod-like nature of the particles was highly apparent, as the nCuO rods were quite difficult to integrate with the polymer, perhaps due to high initial agglomeration. The high aspect ratio and specific surface area of the particles also made them difficult to homogenize with the LabRAM mixer; though the mix acceleration indicated mix completion, significant concentration gradients were still noted in the sample after removal from the mixer (see Fig. 18). Final viscosity values were achieved by mixing until the bulk samples became visibly homogeneous, though when examined in thin layers, agglomeration was still noted in the mixture.

Samples of the nCuO were prepared in 5% (7.5g), 10% (15g), and 15% (22.5g) amounts, and used to acquire viscosity measurements. Further investigation with this material will include the use of pre-sonication to improve dispersion in the viscous binder.

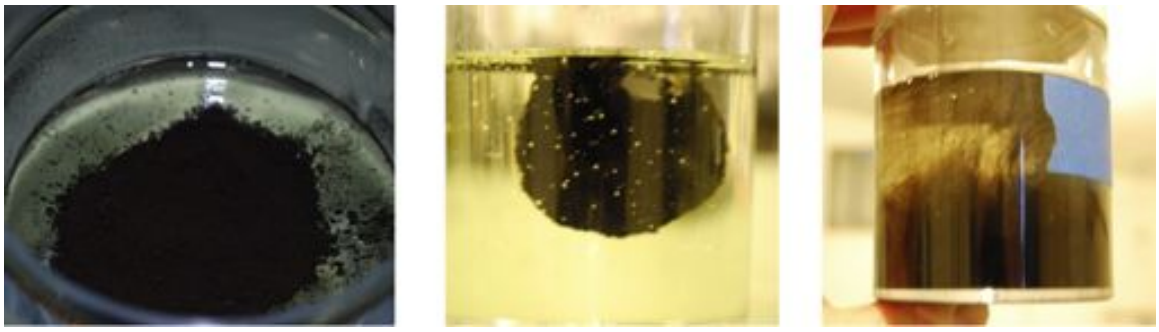

Figure 18: nCuO rods before wetting into HTPB (left), after wetting attempt showing immiscibility (center), after 5 minutes of mixing on LabRAM (right).

4. Preparation of Nanoboron Systems

Nanoboron powder (100 nm nominal diameter) was sourced from American Elements (Los Angeles, CA) for use in preparation of boron-based systems. The dry powder was noted to be very rough feeling as compared to the free-flowing nanoaluminum; mixing of the nanoboron powder also proved extremely difficult. The behavior of the nanoboron powder was similar to that of the nCuO rods, in that it appeared essentially immiscible in the HTPB during pre-wetting. It also proved difficult for the LabRAM to disperse; however, while the nCuO appeared to be mostly de-agglomerated by the LabRAM, the nB showed significant visible agglomeration after 5 minutes of mixing which proved impossible to disperse with further mix time (see Fig. 19). Further research and discussion on the behavior of nanoboron indicates that a treatment of the particles with ammonia solution prior to incorporation into the HTPB may lead to a more successful mixing process; however, this process has not yet been attempted. Sonication of the particles prior to HTPB integration also remains to be investigated.

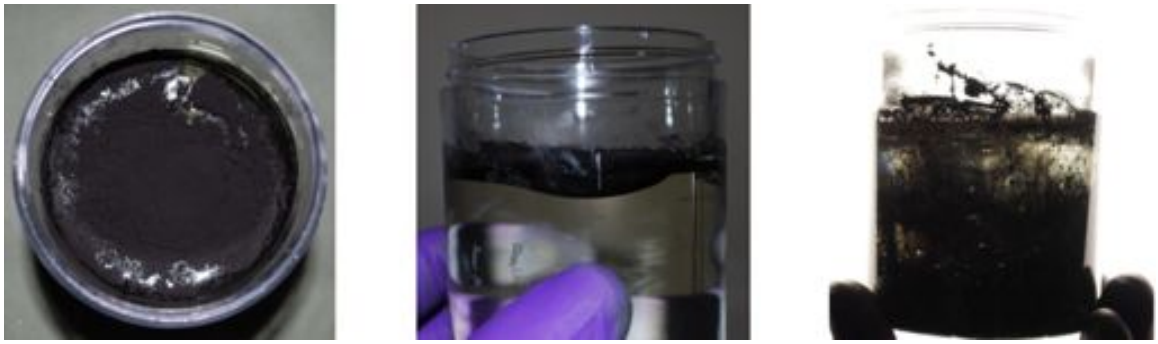

Figure 19: nB powder weighed into HTPB sample (left), after attempts to wet powder into HTPB (center), after extended mixing on LabRAM showing agglomeration (right).

E. Sample Characterization

Following each successful mixing process, all samples were characterized via viscosity measurement. In addition, the nanoaluminum samples were studied further with x-ray and electron microscopy techniques.

1. Viscometry

Mixed samples underwent viscosity measurements immediately after the mixing process. The viscometer selected for this project was the DV-II+Pro model HB, manufactured by Brookfield Engineering Laboratories. The viscometer was used with the HB-1 or HB-2 spindle, depending on the mixture viscosity, and the motor speed adjusted to provide a torque reading as close to full scale as possible such as to maximize measurement precision.

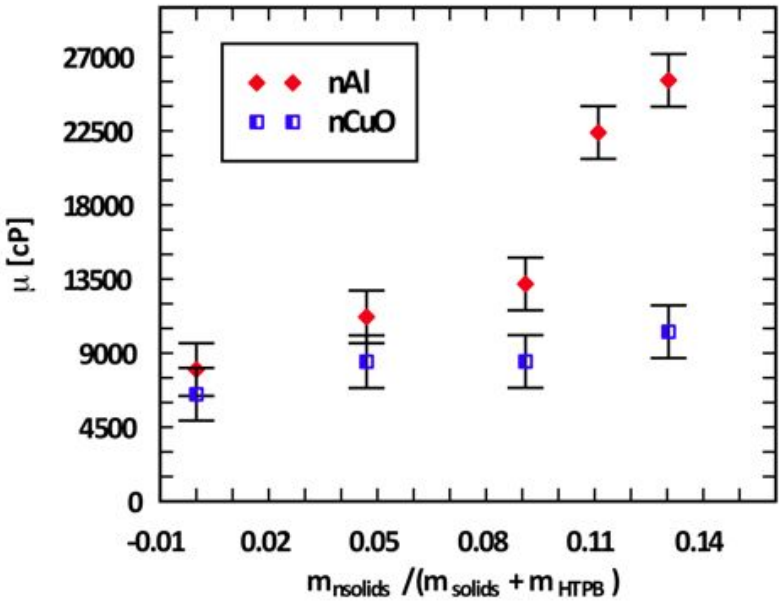

Figure 20: Viscometry results for nAl powder and CuO nanorod mixtures as a function of concentration.

A direct comparison between the viscosities of the aluminum nanoparticles and copper oxide nanorods appears in Fig. 20. The aluminum shows a higher viscosity than the nanorods, likely due to their better dispersion state; the nanorods created a mixture viscous enough to prevent full dispersion, and thus presented a reduced effective surface area to the polymer.

2. SEM Imaging

Samples containing aluminum nanoparticles were also selected to be imaged using a scanning electron microscope to provide further examination of their dispersion quality and to provide a basis for comparison with the numerical models. Representative images for the various concentrations are presented in Fig. 21.

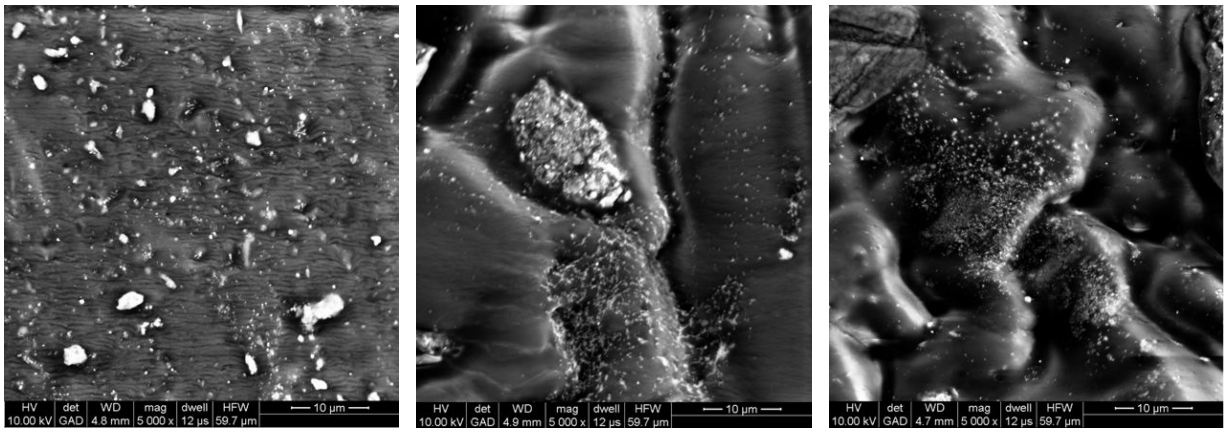

(a) 5% nAl (b) 10% nAl (c) 15% nAl

Figure 21: SEM images for varying weight concentrations of nAl in HTPB. All images contain significant agglomerations on the milli- or micro-scale, with small micro-scale agglomerations appearing at higher mass fractions

SEM imaging illustrates the benefit to dispersion of increased nanoparticle concentration in the mixture; The 5% nominal mixture appears with smoothest topology, as it was cured with a higher NCO:OH ratio, thus providing a stiffer surface for SEM and improving beam resistance. More smaller agglomerates are noted in the 5% mixture, while fewer, larger agglomerates separated by pockets of well-mixed material are present in the 10% and 15% mixes. The 10% and 15% mixes appear to contain higher concentrations of micron- and submicron-size agglomerates, as predicted by the DPD modeling; however, these images are an order of magnitude larger in scale than the DPD simulations illustrate. Though all concentrations appear to exhibit agglomeration to some extent, the mixtures with higher loading exhibit larger pockets of deagglomerated material. This bodes well for future mixes containing additional solids (e.g., burn rate modifiers or additional oxidizers), as it appears that the additional solids help crush the agglomerates during the mixing process.

3. SAXS Characterization

X-ray measurements were taken using a Brukker AXS GADDS diffractometer with a Cu Kα source in an attempt to gather data on the dispersion quality of the prepared samples. A 5% nominal sample was selected for analysis, as the low metals loading provided the best chance for a successful measurement in transmission. The results are presented in Fig.s 22 and 23.

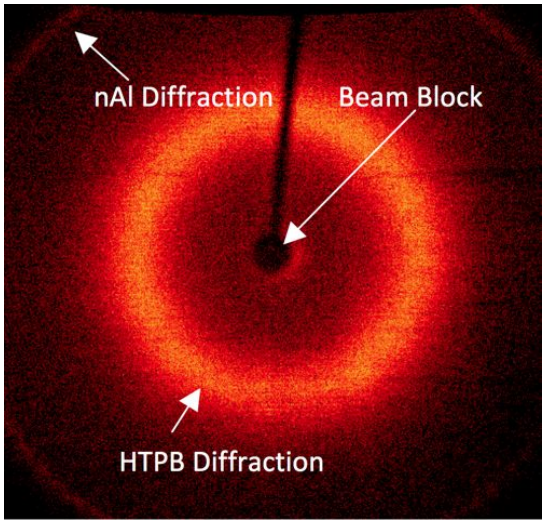

Figure 22: Raw image obtained from x-ray analysis of 5% nAl-containing sample.

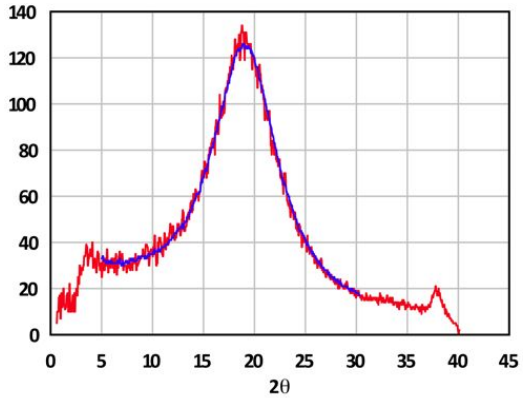

Figure 23: Integrated intensity as a function of scattering angle for 5% nAl-containing sample.

The broad peak in Fig. 23 is generated by the amorphous HTPB molecules; the smaller peak at $2\theta = 38.5°$ corresponds to the aluminum diffraction generated by the Cu Kα beam. Unfortunately, due to the wavelengths it generates, the Kα source is unable to discern agglomeration of 80 nm particles at values of

$2\theta < 0.1°$, and thus no agglomeration is visible in the generated data; any agglomeration is hidden by the beam block and beam spot at the center of the image. A different x-ray source must be used for further investigation of agglomeration on a nano scale.

IV. Conclusions & Future Work

In this paper, we have developed and validated several systems for predicting and creating nanoparticle-containing composite polymer systems. In particular, a phase diagram for predicting disperse *vs.* agglomerated systems was developed using numerical methods, and several methods of creating such systems investigated for practical application. The combination of numerical and experimental results has allowed the identification of several pathways for improvement in dispersion techniques. Future work will include development of "tethered" nanoparticles coated in strings of energetic molecules, identification of appropriate coatings to enable further work with nanoboron, and additional simulations which continue to identify energy and mass fraction boundaries for creation of disperse systems.

Acknowledgments

The team is indebted to Paul Redner and Deepak Kapoor of ARDEC for their assistance and financial support under USACC contract W15QKN-10-C-0020.

References

[1]Galfetti, L., De Luca, L., Severini, F., Meda, L., Marra, G., Marchetti, M., Regi, M., and Bellucci, S., "Nanoparticles for solid rocket propulsion," *J. Phys.: Condens. Matter*, Vol. 18, 2006, pp. S1991–S2005.

[2]Dokhan, A., Seitzman, J., Price, E., and Sigman, R., "The effects of Al particle size on the burning rate and residual oxide in aluminized propellants," *37th AIAA/ASME/SAE/ASEE Joint Propulsion Conf. and Exhibit*, AIAA, Salt Lake City, UT, 2001, pp. 1–12.

[3]Yetter, R., Risha, G., and Son, S., "Metal particle combustion and nanotechnology," *Proceedings of the Combustion Institute*, Jan 2009.

[4]Smith, G. and Paul, W., "United Atom Force Field for Molecular Dynamics Simulations of 1,4-Polybutadiene Based on Quantum Chemistry Calculations on Model Molecules," *J. Phys. Chem. A*, Vol. 102, 1998, pp. 1200–1208.

[5]Smith, G., W. Paul, M. M., L. Willner, D. R., Qiu, X. H., and Ediger, M. D., "Molecular Dynamics of a 1,4-Polybutadiene Melt. Comparison of Experiment and Simulation," *Macromolecules*, Vol. 32, 1999, pp. 8857–8865.

[6]Byutner, O. and Smith, G., "Prediction of the Linear Viscoelastic Shear Modulus of an Entangled Polybutadiene Melt from Simulation and Theory," *Macromolecules*, Vol. 34, 2001, pp. 134– 139.

[7]Hooper, J., Bedrov, D., Smith, G., Hanson, B., Borodin, O., Dattelbaum, D. M., and Kober, E. M., "A molecular dynamics simulation study of the pressure-volume temperature behavior of polymers under high pressure," *J. Chem. Phys.*, Vol. 130, 2009, pp. 144904.

[8]Millett, J. C. F., Bourne, N. K., and Akhavan, J., "The response of hydroxy-terminated polybutadiene to one-dimensional shock loading," *J. Appl. Phys.*, Vol. 95, 2004, pp. 4722.

[9]Plimpton, S., "Fast Parallel Algorithms for Short-Range Molecular Dynamics," *J. Comp. Phys.*, Vol. 117, 1995, pp. 1.

[10]Li, Y. and Mattice, W., "Atom Based Modeling of Amorphous 1,4-cis-Polybutadiene," *Macromolecules*, Vol. 25, 1992, pp. 4942.

[11]Jin, R., Song, K., and Hase, W., "Molecular Dynamics Simulations of the Structures of Alkane/Hydroxylated r-Al_2O_3 Interfaces," *J. Phys. Chem. B*, Vol. 104, 2000, pp. 2692.

[12]Español, P., "Smoothed particle hydrodynamic model for viscoelastic fluids with thermal fluctuations," *Physical Review E*, 2009, pp. 79.

[13]ResoDyn Corporation, Butte, MT, *LabRam ResonantAcoustic Mixer Manual*.